Electronic Supplementary Material (ESI) for Sustainable Energy & Fuels.
This journal is © The Royal Society of Chemistry 2022

Electronic Supporting Information for the manuscript:

"Oxidative polymerization of triarylamines: a promising route to low-cost hole transport materials for efficient perovskite solar cells"

Olga A. Kraevaya, Alina F. Latypova, Alexandra A. Sokolova, Anastasiya A. Seleznyova, Nikita A. Emelianov, Nikita A. Slesarenko, Vitaliy Yu. Markov, Lyubov A. Frolova and Pavel A. Troshin*

Table S1. Molecular weight distribution for PTAAs

Polymer	M_n,kDa*	M_w, kDa*	M_w/M_n*
P1	8.3	15.8	1.9
P2	8.8	15.7	1.8
P3	9.6	17.0	1.8
Commercial PTAA*	15.4	26.3	1.7

*Calculated from gel-permeation chromatography (GPC). Measurements carried out using chlorobenzene as the eluent and calibrated *vs.* polystyrene standards.

***PTAA* is poly[bis(4-phenyl)(2,4,6-trimethylphenyl)amine] by Ossila.

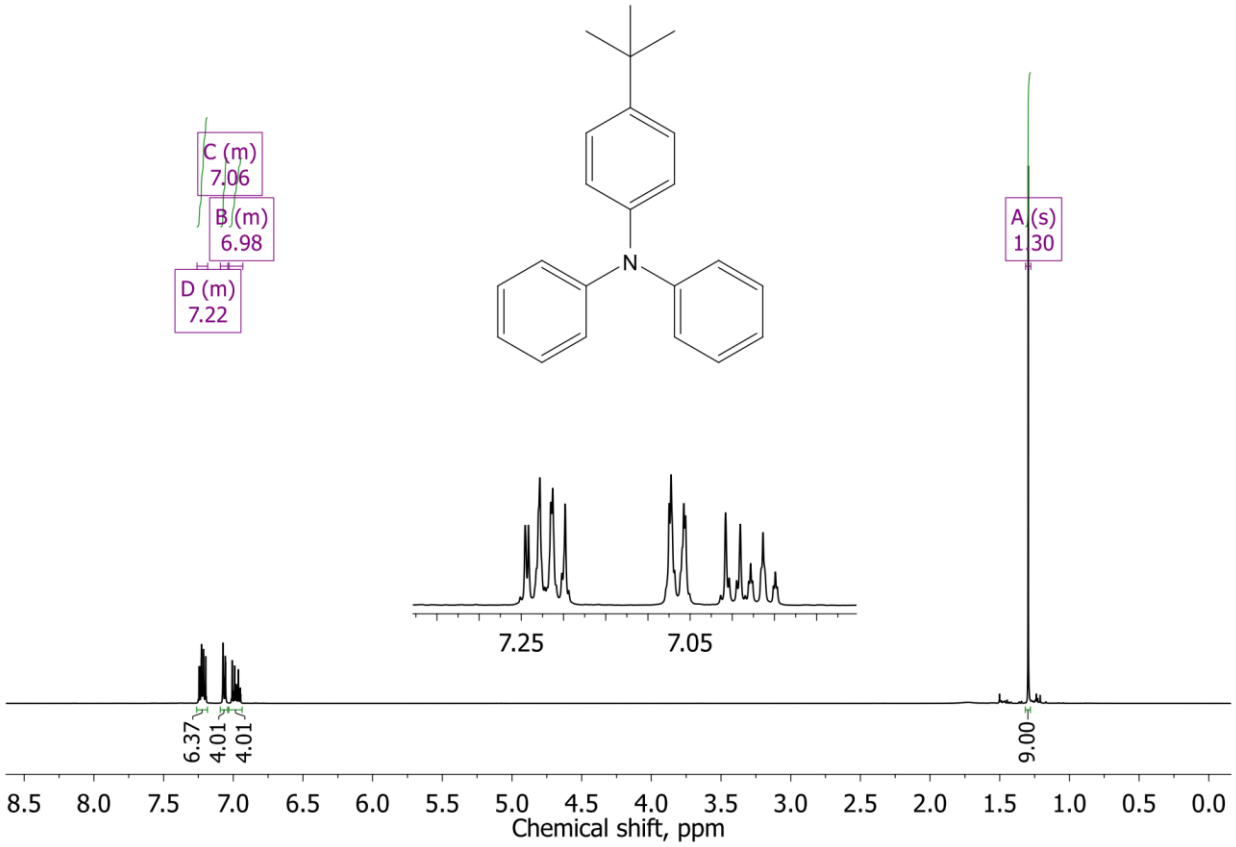

Figure S1. ^{1}H NMR spectrum of compound **2**

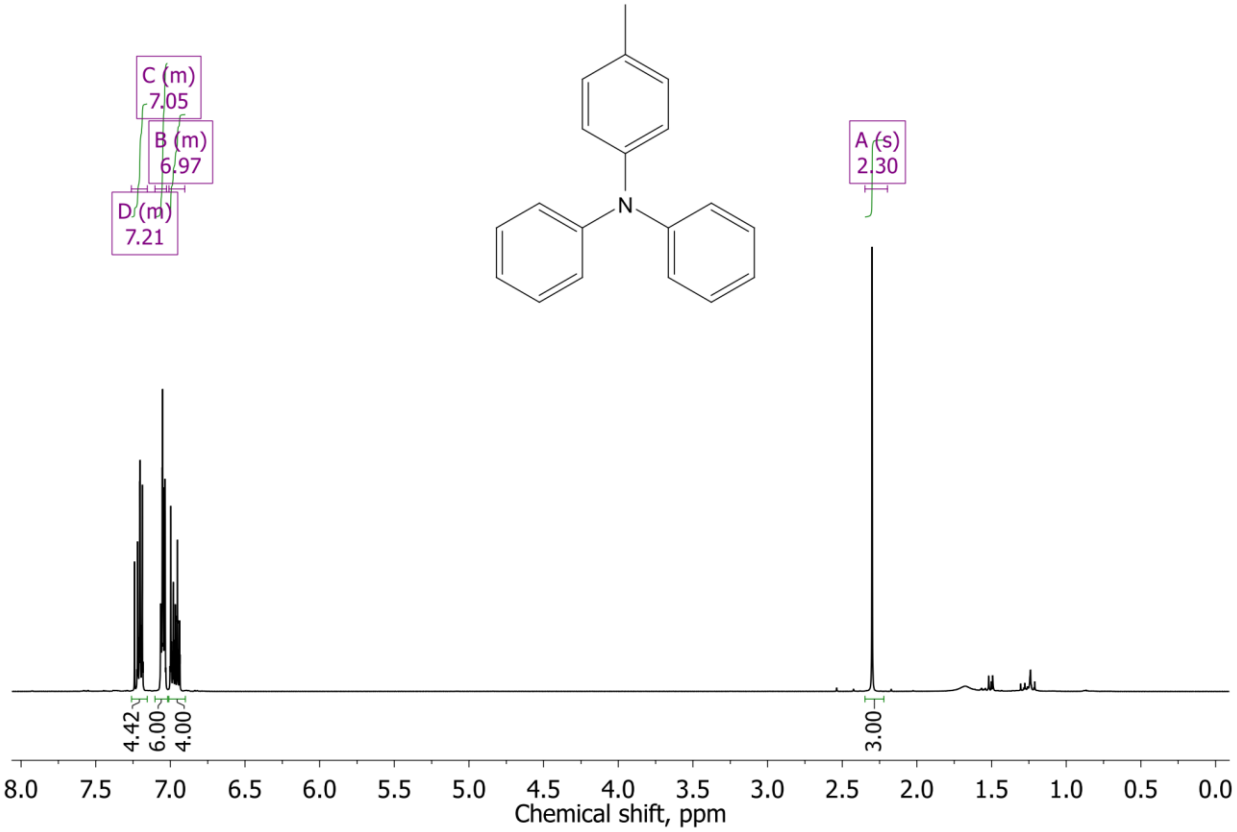

Figure S2. ^{1}H NMR spectrum of compound **3**

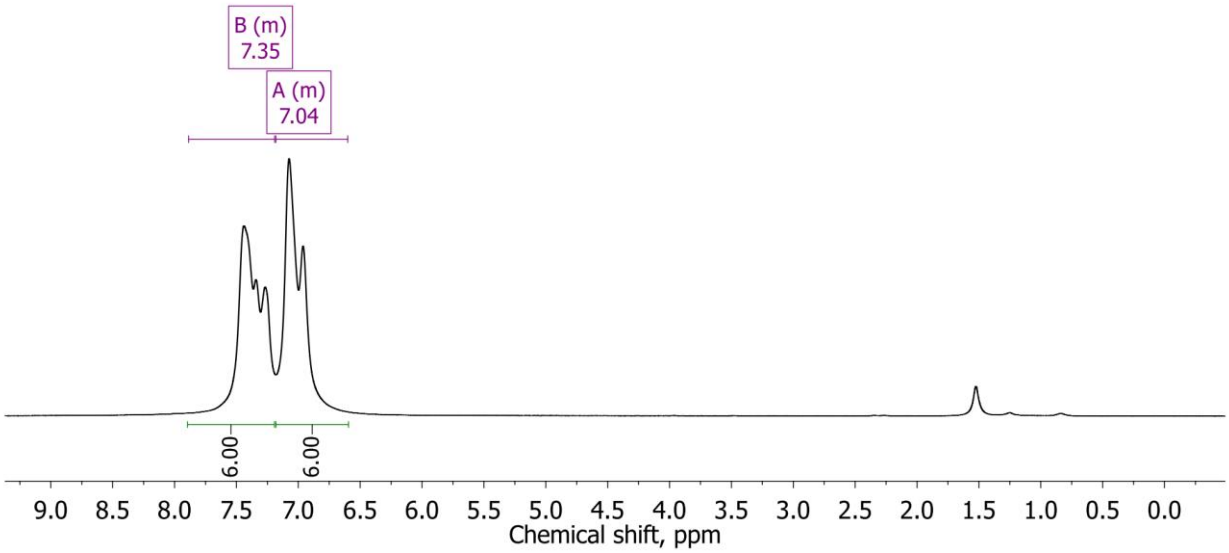

Figure S3. ^{1}H NMR spectrum of **P1**

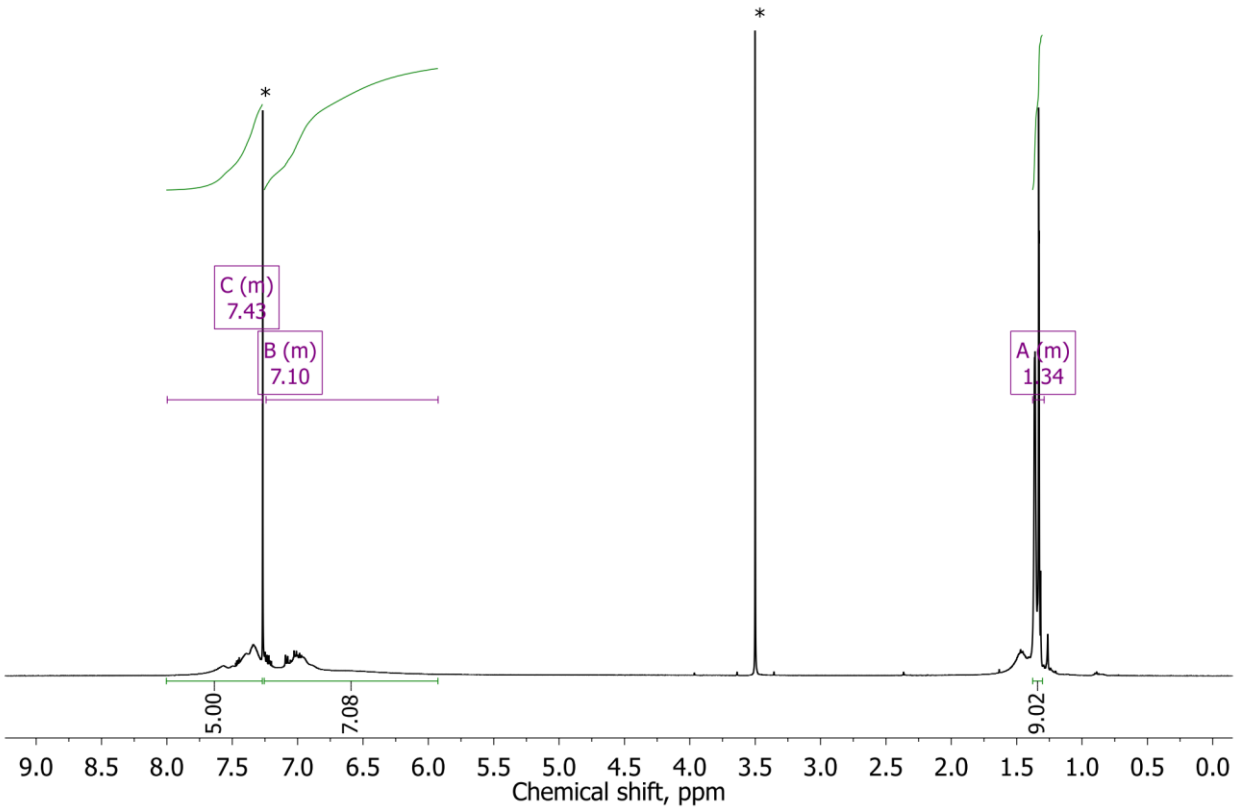

Figure S4. ^{1}H NMR spectrum of **P2** (* denotes signals of $CHCl_3$ and MeOH)

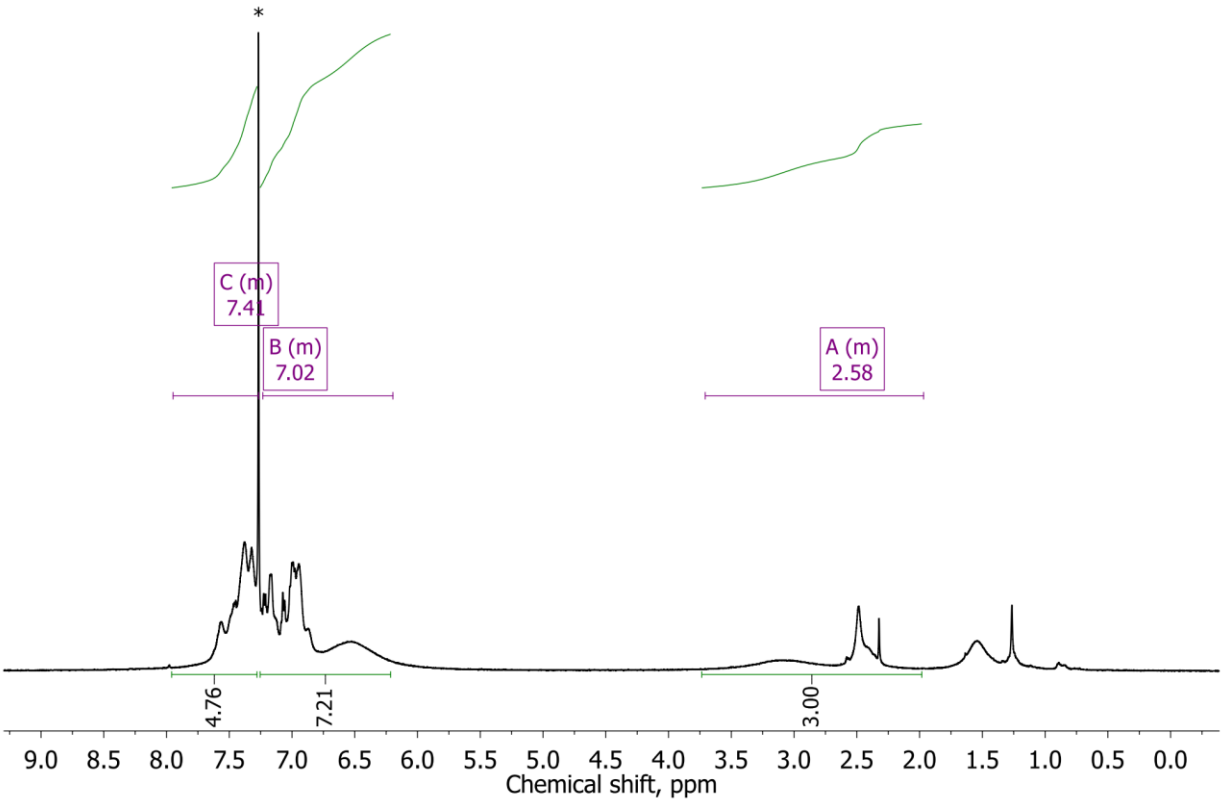

Figure S5. ^{1}H NMR spectrum of **P3** (* denotes signal of $CHCl_3$)

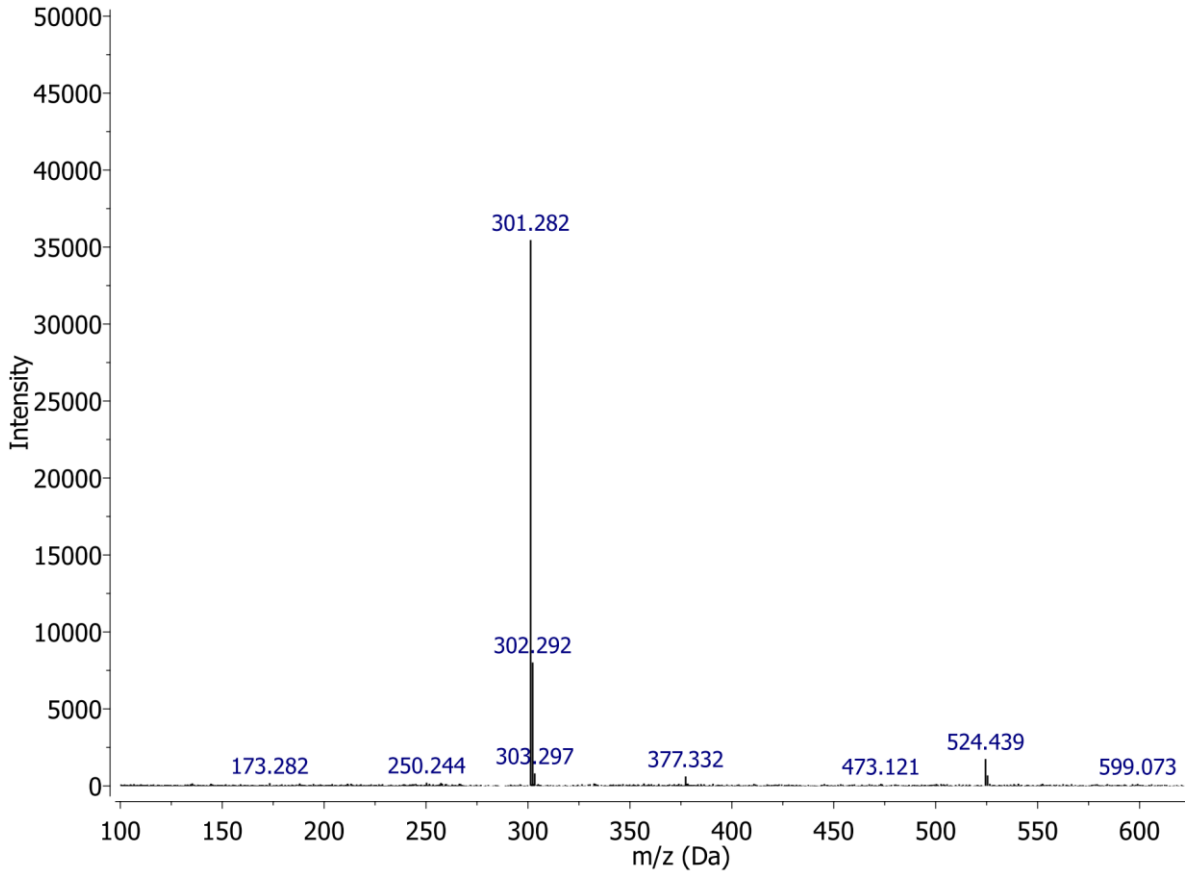

Figure S6. MALDI mass spectrum of compound **2**

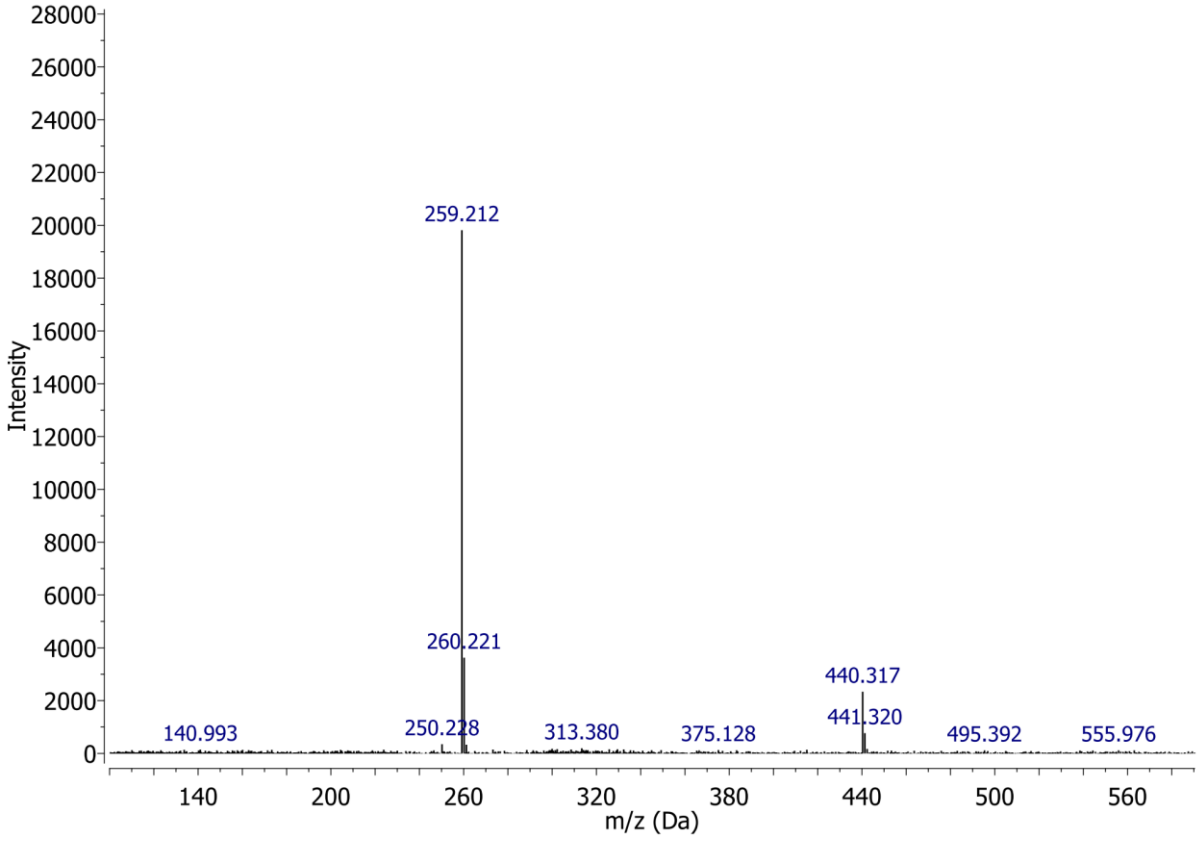

Figure S7. MALDI mass spectrum of compound **3**

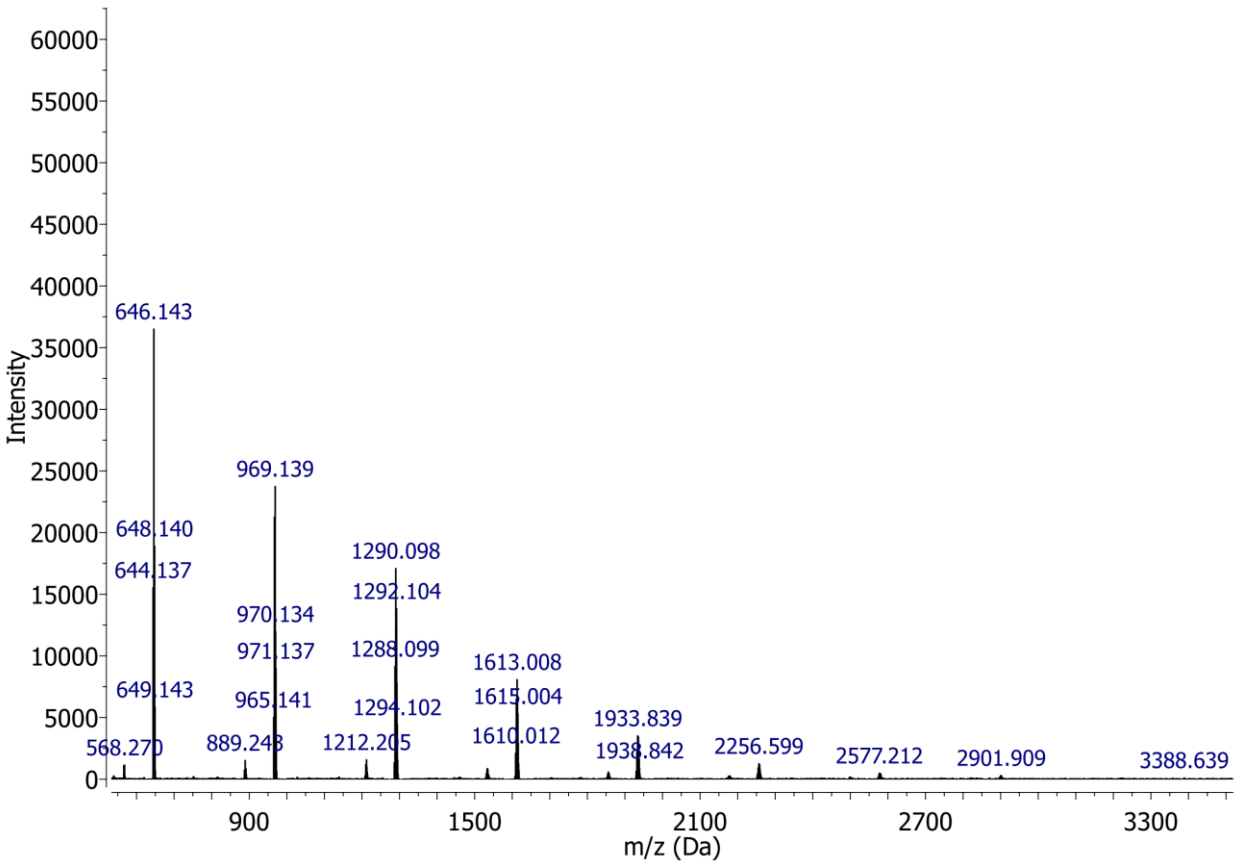

Figure S8. MALDI mass spectrum of **P1**

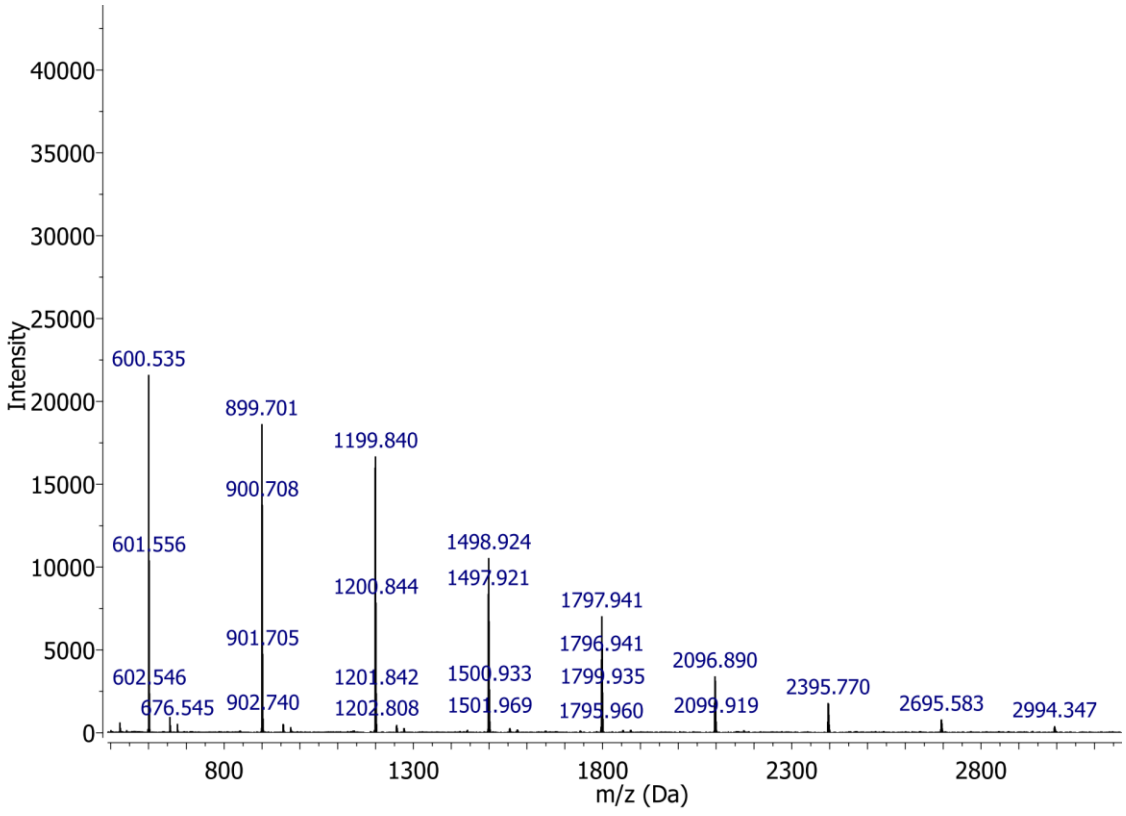

Figure S9. MALDI mass spectrum of **P2**

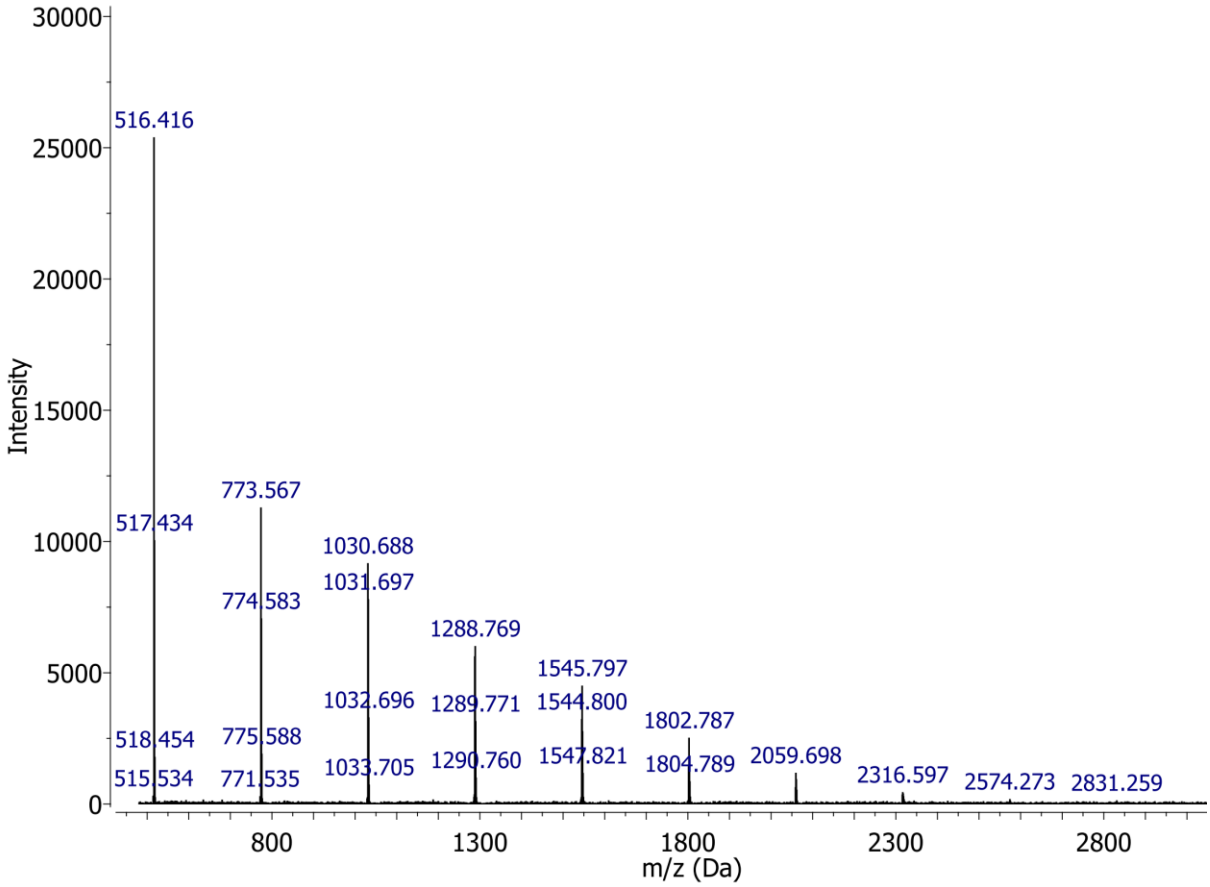

Figure S10. MALDI mass spectrum of **P3**

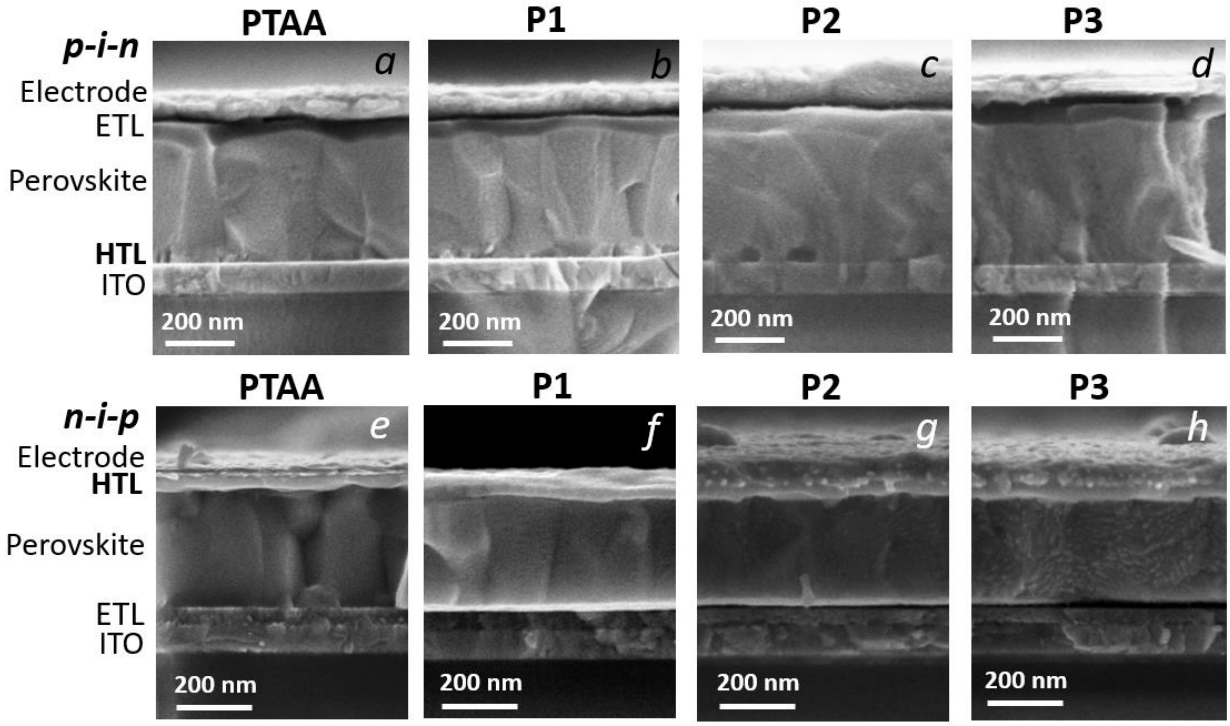

Figure S11. Cross-section SEM images of the p-i-n and n-i-p perovskite solar cells comprising different HTMs: *PTAA* (a, e), **P1** (b, f), **P2** (c, g) and **P3** (d, h).

Table S2. The average* and the best (in brackets) values of power conversion efficiency (PCE), open-circuit voltage (V_{OC}), short-circuit current density (J_{SC}), and fill factor (*FF*) of the ITO/SnO_2/PCBA/$MAPbI_3$/HTM/VO_x/Ag devices comprising different HTMs.**

HTM	Scan direction	V_{OC}, V	J_{SC}, mA cm^{-2}	*FF*, %	PCE, %
PTAA	Forward	(1.049) 1.035 ± 0.014	(23.1) 22.7± 0.4	(72.7) 70.9 ± 1.8	(17.6) 16.7 ± 0.9
	Reverse	(1.042) 1.024 ± 0.018	(23.2) 22.6± 0.6	(71.4) 69.4 ± 2.0	(17.2) 16.9 ± 0.3
P1	Forward	(1.040) 1.019 ± 0.021	(23.4) 23.0 ± 0.4	(67.0) 64.9± 2.1	(16.03) 15.2 ± 0.9
	Reverse	(1.046) 1.028 ± 0.018	(23.3) 22.9 ± 0.4	(65.4) 63.1 ± 2.3	(15.5) 14.9 ± 0.6
P2	Forward	(1.041) 1.030 ± 0.011	(23.3) 22.8 ± 0.5	(74.0) 72.9 ± 2.1	(18.1) 17.1 ± 1.0
	Reverse	(1.033) 1.019 ± 0.014	(23.4) 22.9 ± 0.5	(73.0) 70.8 ± 2.2	(17.7) 16.5 ± 1.3
P3	Forward	(1.053) 1.030 ± 0.023	(23.2) 22.5 ± 0.7	(76.2) 73.7 ± 2.5	(18.6) 17.1 ± 1.5
	Reverse	(1.043) 1.016 ± 0.017	(23.3) 22.5 ± 0.8	(75.5) 73.2 ± 2.3	(18.4) 16.7 ± 1.7

Notes: *Average values (± standard deviation from the mean) obtained for a batch of 12 devices. ** The *J*–*V* curves were measured in forward and reverse directions with the scan rate of 0.01 V/s

Table S3. The average* and the best (in brackets) values of power conversion efficiency (PCE), open-circuit voltage (V_{OC}), short-circuit current density (J_{SC}), and fill factor (*FF*) of the ITO/HTM /$Cs_{0.1}MA_{0.15}FA_{0.75}PbI_3$/PCBM/BCP/Ag devices comprising different HTMs.**

HTM	Scan direction	V_{OC}, V	J_{SC}, mA cm^{-2}	*FF*, %	PCE, %
PTAA	Forward	(1.046) 1.034 ± 0.012	(23.3) 22.8± 0.5	(81.7) 80.1 ± 1.6	(19.9) 18.8 ± 1.1
	Reverse	(1.055) 1.042 ± 0.013	(23.2) 22.7 ± 0.5	(80.9) 78.8 ± 2.1	(19.8) 18.8 ± 1.0
P1	Forward	(1.070) 1.050 ± 0.020	(23.3) 22.9 ± 0.4	(78.1) 75.9 ± 2.2	(19.5) 18.4 ± 1.1
	Reverse	(1.073) 1.056 ± 0.017	(23.3) 22.8 ± 0.5	(76.9) 74.6 ± 2.3	(19.2) 18.0 ± 1.2
P2	Forward	(1.050) 1.031 ± 0.019	(23.3) 22.8 ± 0.5	(80.4) 78.3 ± 2.1	(19.7) 18.4 ± 1.3
	Reverse	(1.063) 1.042 ± 0.021	(23.2) 22.8 ± 0.4	(79.8) 77.6 ± 2.2	(19.7) 18.4 ± 1.3
P3	Forward	(1.041) 1.016 ± 0.025	(23.6) 23.1 ± 0.5	(81.2) 78.9 ± 2.3	(20.04) 18.5 ± 1.5
	Reverse	(1.038) 1.015 ± 0.023	(23.5) 22.9 ± 0.6	(81.6) 79.5 ± 2.1	(20.10) 18.5 ± 1.6

Notes: * Average values (± standard deviation from the mean) obtained for a batch of 12 devices. ** The *J*–*V* curves were measured in forward and reverse directions with the scan rate of 0.01 V/s

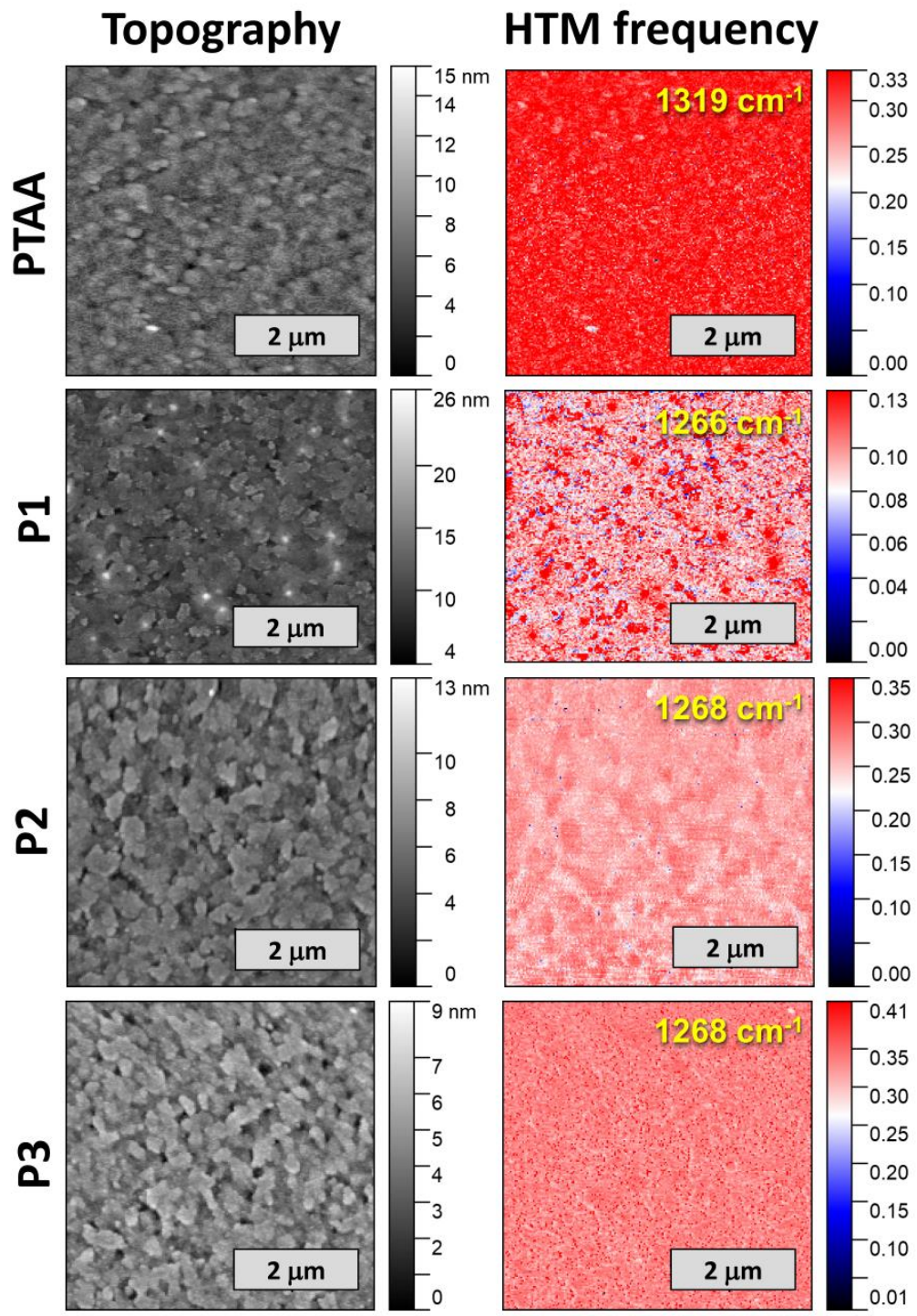

Figure S12. AFM topography (left column), and s-SNOM amplitude images for the glass/HTM samples recorded at the characteristic frequencies of HTM.

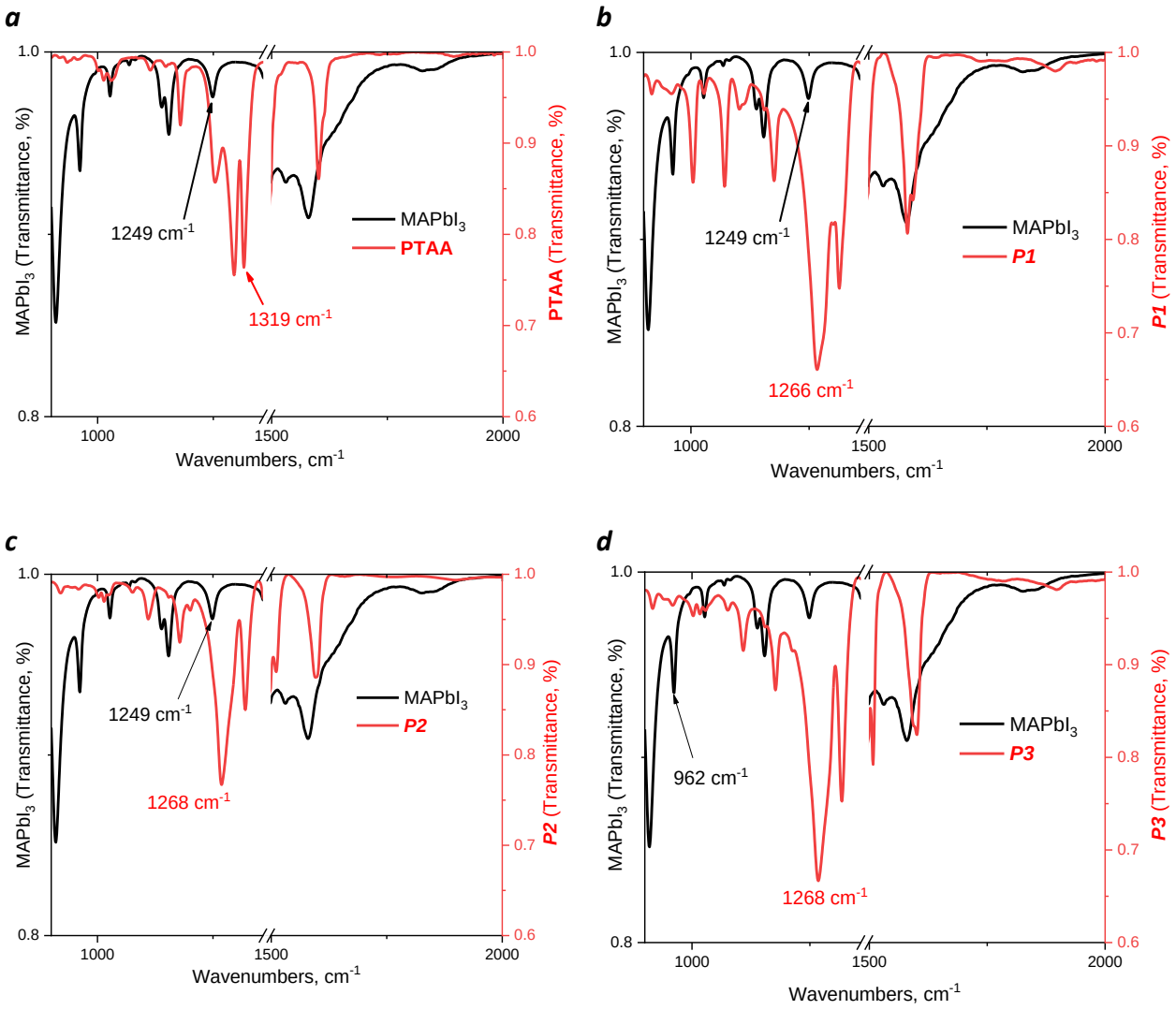

Figure S13. FTIR spectra of commercial *PTAA* (a), **P1** (b), **P2** (c), **P3** (d) and their comparison with FTIR spectrum of $MAPbI_3$

Experimental procedures

NMR spectroscopy

NMR spectra were recorded on Bruker AVANCE III 500 MHz spectrometer in $CDCl_3$.

Mass spectrometry

All mass spectra were acquired using MALDI ionization method on a Bruker AutoFlex Bruker AutoFlex II reflector time-of-flight device equipped with a N_2 laser (337 nm wavelength, 2.5 ns pulse). Trans-2-[3-(4-tert-butylphenyl)-2-methyl-2-propenylidene]malononitrile (DCTB) (≥98%, Sigma-Aldrich) was used as a matrix. The measurements were performed in a positive ion mode.

Preparation of perovskite precursor solutions

For the preparation of 1.4 M $MAPbI_3$ precursor solution, MAI and PbI_2 were dissolved in a mixture of 0.850 mL of DMF and 0.150 mL of NMP. To obtain 1.35 M $MA_{0.1}Cs_{0.15}FA_{0.75}PbI_3$ precursor solution, CsI, MAI, FAI, and PbI_2 were dissolved in a mixture of 0.200 mL of anhydrous DMSO and 0.800 mL of anhydrous DMF. The precursor solutions were heated at 80°C for an hour and filtered through PTFE syringe filters (0.45 μm) prior spin-coating.

Fabrication of n-i-p perovskite solar cells

ITO glass substrate (Kintec, 15 Ω sq^{-1}) was cleaned with deionized water, acetone, and isopropanol in an ultrasonic bath. The tin dioxide layer was obtained by spin-coating 10% aqueous tin dioxide suspension (Alfa-Aesar) at 4000 rpm for 40 s followed by annealing at 175°C in air for 15 minutes. Substrates were transferred inside a nitrogen glove box and all subsequent steps were performed there. The solution of PCBA in chlorobenzene (0.1 mg mL^{-1}) was spin coated at 3500 rpm for 30 seconds. The obtained films were annealed at 100 °C within 10 minutes. $MAPbI_3$ precursor solution (70 μL) was spin-coated at 4000 rpm and then quenched with 130 μL of toluene 18 seconds later to produce the active layer with 200–250 nm thickness. The deposited films were annealed for 10 minutes at 100°C on a hotplate. HTL was deposited by spin-coating of the HTM polymer solution in chlorobenzene (*PTAA*: 6 mg mL^{-1}; P1: 9 mg mL^{-1}; P2, P3: 8 mg mL^{-1}) at 1000 rpm (PTAA, P2 and P3) or 2000 rpm (P1) for 60 s. Electron blocking layer of vanadium oxide (VO_x) with the thickness of 30 nm was deposited by vacuum evaporation. Top Ag electrodes (120 nm) were thermally evaporated through a shadow mask in high vacuum (5×10^{-6} Torr). Active areas of the devices were in the range of 0.4–0.5 cm^2.

Fabrication of p-i-n perovskite solar cells

ITO glass substrates were cleaned as described above. The solution of HTM (*PTAA* or P1-P3) in chlorobenzene (2.5 mg mL^{-1}) was spin-coated at 3500 rpm for 60 s on the ITO substrates, followed by thermal annealing at 160 °C for 15 min inside glove box. The perovskite films were deposited by spin-coating $MA_{0.1}Cs_{0.15}FA_{0.75}PbI_3$ precursor solution at 4000 rpm for 60 s. The solution was quenched by 35 μL of chlorobenzene dripped onto the film at 33rd second. Obtained perovskite films were annealed at 120 °C for 2 min. Then a PCBM precursor solution

(30 mg mL^{-1} in chlorobenzene) was spin-coated on top of the perovskite layer at 2000 rpm for 50 s. BCP hole-blocking layer (3 nm) was deposited by thermal evaporation. Finally, Ag (120 nm) electrodes were evaporated through a shadow mask in high vacuum (5×10^{-6} Torr) to produce devices with the area of 0.45 cm^2.

Characterization of the devices

The devices were characterized by *J-V* and EQE measurements inside MBraun glove box under inert nitrogen atmosphere. The *J–V* characteristics of the devices were registered using Advantest R6240A source-measurement units and KHS Steuernagel Lichttechnik solar simulator as a source of the simulated 100 mW cm^{-2} AM1.5G illumination. The light flux was checked with a calibrated silicon diode. Obtained J_{SC} values were compared with the values derived from the integration of the EQE spectra against AM1.5G spectrum. The EQE measurements were performed under ambient conditions. The EQE setup was equipped with 300 W Xenon lamp, automatic monochromator (LOMO instruments), SR510 lock-in amplifier combined with SR540 optical chopper (Stanford Research Instruments).